PCCP

Dynamic Article Links ►

Cite this: DOI: 10.1039/c0xx00000x

www.rsc.org/xxxxxx

PAPER

Effects of HF content in the $(FH)_nF^-$ anion on the formation of ionic plastic crystal phases of *N*-ethyl-*N*-methylpyrrolidinium and *N*,*N*-dimethylpyrrolidinium fluorohydrogenate salts

Ryosuke Taniki, Kazuhiko Matsumoto* and Rika Hagiwara

Received (in XXX, XXX) Xth XXXXXXXXX 20XX, Accepted Xth XXXXXXXXX 20XX
DOI: 10.1039/b000000x

Fluorohydrogenate salts based on *N*-ethyl-*N*-methylpyrrolidinium (EMPyr$(FH)_nF$) and *N*,*N*-dimethylpyrrolidinium (DMPyr$(FH)_nF$) cations were synthesized, and the effects of the HF content *n* in EMPyr$(FH)_nF$ ($1.0 \le n \le 2.3$) and DMPyr$(FH)_nF$ ($1.0 \le n \le 2.0$) on their thermal and structural properties were discussed, focusing on the characterization of ionic plastic crystal (IPC) phases. Several solid phases (IPC (I) and IPC (II) phases, and crystal phases of EMPyr$(FH)_1F$, EMPyr$(FH)_2F$, and EMPyr$(FH)_3F$) are observed in the EMPyr$(FH)_nF$ system. The IPC (I) phase has an NaCl-type structure and is composed of $EMPyr^+$ cations and $(FH)_nF^-$ (n = 1, 2, and 3) anions randomly occupying the anion positions in the lattice over a wide range of *n* values in $(FH)_nF^-$. Melting point of EMPyr$(FH)_nF$ in the range $1.8 \le n \le 2.3$ is maximal at $n = 2.0$, whereas it increases with decrease in *n* in the range $1.0 \le n \le 1.2$. Furthermore, in the range $1.3 \le n \le 1.7$, the solid phase is regarded as IPC phase (IPC (II)), and their melting points are nearly constant (260–270 K). In DMPyr$(FH)_nF$ system, the IPC (I') phase and crystal phases of DMPyr$(FH)_1F$ and DMPyr$(FH)_2F$ were observed. Although the IPC (I') phase has an NaCl-type structure, similar to the IPC (I) phase of EMPyr$(FH)_nF$, it has higher ordering compared to the IPC (I) phase. The melting point of DMPyr$(FH)_nF$ increases monotonously with decreasing *n* but disappears in the small *n* region where the salt decomposes below the melting point.

Introduction

Ionic compounds based on non-aromatic cations, such as pyrrolidinium, tetraalkylammonium, tetraalkylphosphonium, and trialkylsulfonium cations, sometimes exhibit plastic properties around room temperature.[1-8] These materials based on ionic species have been known as ionic plastic crystals (IPCs), and IPCs containing organic species are called organic IPCs. The first systematic study on an organic molecule-containing plastic crystal (PC) phase was carried out by Timmermans in 1961.[9] Such a phase is an intermediate state formed by first-order solid–solid phase transitions below the melting point. The constituent molecules or ions in the PC phase are characterized by rotational motion and long-range positional order. This rotational behavior contributes to the formation of defects and gives rise to liquid-like features such as fast diffusion of the constituent ions or doped ions and plastic mechanical properties.[10,11] Timmermans proposed a general rule to organic molecules that a PC phase has low entropy of fusion (ΔS_{fus} < 20 J K^{-1} mol^{-1}) because the constituent molecules or ions are rotating in the PC phase, and the entropy change corresponding to the rotational freedom is considered to be very small for the transition from the PC phase to the liquid phase. With increasing temperature, the constituent molecules or ions start to rotate around at least one molecular axis either suddenly at the phase transition or over a range of temperatures.[4] Rotating motions in the PC phase increase the entropy of the solid state to close to that of the liquid state, rendering a small value of ΔS_{fus} compared to that of a fully ordered crystal.

The IPCs consist entirely of ions and thus have extremely low vapor pressure and non-flammability, which is favorable for improving the safety and reliability of electrochemical devices. The use of IPCs as solid-state electrolytes offers prevention of electrolyte leakage, flexible and thin configuration of devices, volumetric stability during the cell operation, and easy packing and handling.[7,12-14] The values of solid-state ionic conductivity are usually between 10^{-3} and 10^{0} mS cm^{-1} at 298 K, and are appropriate for use in practical applications.[1,5,15-17] As described in a previous study,[18] fluorohydrogenate salts, EMPyr$(FH)_{2.0}F$ ($EMPyr^+$: *N*-ethyl-*N*-methylpyrrolidinium cation) and DMPyr$(FH)_{2.0}F$ ($DMPyr^+$: *N*,*N*-dimethylpyrrolidinium cation), exhibit an IPC phase with high ionic conductivity around room temperature (14.4 mS cm^{-1} at 288 K for EMPyr$(FH)_{2.0}F$ and 10.3 mS cm^{-1} at 298 K for DMPyr$(FH)_{2.0}F$, respectively).[18] A recent work confirmed that the IPC phase of DMPyr$(FH)_{2.0}F$ works as an electrolyte in electrochemical capacitors with high capacitances.[19] The temperature range of the IPC phase is determined by crystal-to-IPC and IPC-to-liquid transitions, being 236 and 303 K for EMPyr$(FH)_{2.0}F$ and 258 and 325 K for DMPyr$(FH)_{2.0}F$, respectively. The utilization of these salts as

electrolytes at high temperatures (e.g., 373 K) is difficult owing to the narrow range of temperatures over which the IPC phase is observed. According to previous works, the high-temperature limit of the IPC phase can be increased by modifying the structures of the component ions without increasing the low-temperature limit.[2,3,5,10,17,20-23] In the cases of fluorohydrogenate salts, the melting point depends on the HF content n in fluorohydrogenate anions ($(FH)_nF^-$).[24-26] The n value of the vacuum-stable salt is controlled by the elimination of HF at elevated temperatures. The anionic species in fluorohydrogenate salts are FHF^- and $(FH)_2F^-$ in $1.0 \leq n \leq 2.0$ and are $(FH)_2F^-$ and $(FH)_3F^-$ in $2.0 \leq n \leq 3.0$. For example, the overall trends in the melting points of $EMIm(FH)_nF$ ($EMIm^+$; 1-ethyl-3-methylimidazolium cation) and $C_{12}MIm(FH)_nF$ ($C_{12}MIm^+$; 1-dodecyl-3-methylimidazolium cation) indicate that a decrease in n increases the melting point.[25,26] The same trend was observed for alkali metal fluoride-HF systems: the liquidus line increases with decreasing n, though several eutectic points are observed.[27-29]

Unlike dialkylimidazolium fluorohydrogenate systems, the thermal and structural properties of dialkylpyrrolidinium fluorohydrogenate systems with different n values have not been studied so far. As this is important for understanding the thermal and structural properties of the IPC phase of dialkylpyrrolidinium salts and IPC phases in general, in this study, the effects of HF content n in $(FH)_nF^-$ in $EMPyr(FH)_nF$ ($1.0 \leq n \leq 2.3$) and $DMPyr(FH)_nF$ ($1.0 \leq n \leq 2.0$) on the thermal and structural properties of these salts are discussed.

Experimental

Synthesis

The starting $EMPyr(FH)_nF$ ($n > 2.3$) was prepared by a reaction of EMPyrCl (Yoyu Lab.) and excess HF as described in a previous report.[18] Pumping of $EMPyr(FH)_nF$ ($n > 2.3$) at 298 and 393 K resulted in $EMPyr(FH)_{2.3}F$ and $EMPyr(FH)_{1.2}F$, respectively. The bifluoride salt, $EMPyr(FH)_{1.0}F$, was prepared by the neutralization of EMPyrOH with hydrofluoric acid. The EMPyrOH was prepared by passing aqueous EMPyrCl solution through a column filled with an anion exchange resin (OH^- type, Dowex Monosphere 550A). The concentration of hydrofluoric acid was adjusted to 1 M HF (aq) by diluting commercial aqueous HF (Wako Pure Chemical Industries, 46%) with distilled water. The HF content in $EMPyr(FH)_nF$ ($1.0 < n < 2.3$) was controlled by mixing $EMPyr(FH)_{2.3}F$ with $EMPyr(FH)_{1.2}F$ or $EMPyr(FH)_{1.0}F$. The HF contents of the obtained salts were confirmed by titration using 0.1029 M aqueous NaOH solution (Aldrich). Karl-Fischer measurements showed the water contents of $EMPyr(FH)_{2.3}F$ and $EMPyr(FH)_{1.0}F$ were around 100 and 250 ppm, respectively. The anionic species in $EMPyr(FH)_nF$ (FHF^-, $(FH)_2F^-$, and $(FH)_3F^-$) were identified by infrared spectroscopy, as shown in Fig. S1, where the absorption bands of ~1250 (m) cm^{-1} for FHF^-, ~1800 (s), ~1990 (m) and ~2330 (m) cm^{-1} for $(FH)_2F^-$, and 950 (w) cm^{-1} for $(FH)_3F^-$ agree with those reported previously.[25,30,31]

The fluorohydrogenate salt, $DMPyr(FH)_nF$, was prepared in the same way as $EMPyr(FH)_nF$. Pumping of $DMPyr(FH)_nF$ ($n > 2.0$) at 298 and 393 K resulted in $DMPyr(FH)_{2.0}F$ and $DMPyr(FH)_{1.0}F$, respectively. The HF content in $DMPyr(FH)_nF$ ($1.0 < n < 2.0$) was controlled by mixing $DMPyr(FH)_{1.0}F$ with $DMPyr(FH)_{2.0}F$. The HF contents of the obtained salts were confirmed by titration using 0.1029 M aqueous NaOH solution. Karl-Fischer measurements showed the water contents of $DMPyr(FH)_{2.0}F$ and $DMPyr(FH)_{1.0}F$ were around 100 ppm. The anionic species in $DMPyr(FH)_nF$ (FHF^- and $(FH)_2F^-$) were identified by infrared spectroscopy (Fig. S2) as in the case of $EMPyr(FH)_nF$.[25,30,31] The obtained IPCs are flexible as they can be easily shaped to thin and self-standing film in Fig. 1.

Analysis

Water content was measured using a Karl Fischer moisture analyzer (MKC-510N, Kyoto Electronics Mfg. Co.). Infrared spectra were recorded on an FT-IR spectrometer (FTS-155, Bio-Rad Laboratories) at room temperature. The samples were sandwiched between a pair of AgCl windows fixed in a stainless airtight cell under a dry argon atmosphere. Thermal decomposition temperatures were measured by using a differential thermogravimetric analyzer (DTG-60H, Shimadzu). The measurements were performed by using nickel cells under a dry argon gas flow (50 mL min^{-1}). The scan rate was 1 K min^{-1}. The samples were held at 373 K for 1 h to remove water. Thermal analyses for the determination of the melting point and solid–solid phase transition temperature were performed by using a differential scanning calorimeter (DSC-60, Shimadzu). A pressing machine was used to seal the samples in a pressure-resistant cell under a dry argon atmosphere. The scan rate used for the measurements was 5 K min^{-1}, and the measurements were carried out under a dry argon gas flow (50 mL min^{-1}). The samples for powder X-ray diffraction (XRD) analysis were transferred into a quartz capillary under dry argon atmosphere. The capillary was flame-sealed using an oxygen burner and centered on an X-ray diffractometer (R-axis Rapid II, Rigaku) equipped with an imaging plate area detector (employing RAPID XRD 2.3.3 program)[32] and graphite-monochromated MoKα radiation source (0.71073 Å). The φ angle was rotated at a rate of 1° s^{-1}, and the ω and χ angles were fixed at 20° and 0°, respectively, during data collection (1440 s). The sample temperature was controlled by nitrogen flow.

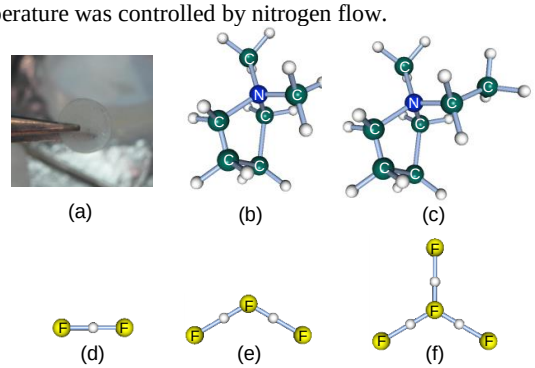

Fig. 1 (a) Photo of an IPC self-standing film of $DMPyr(FH)_{1.0}F$ and structures of (b) $DMPyr^+$, (c) $EMPyr^+$, (d) FHF^-, (e) $(FH)_2F^-$, and (f) $(FH)_3F^-$.

Results and discussion

Thermal and structural properties of $EMPyr(FH)_nF$

Table 1 Summary of the DSC analyses for EMPyr(FH)$_n$F ($1.0 \le n \le 2.3$).

n	T_{s-s}[a] / K	ΔH / kJ mol^{-1}	ΔS / J mol^{-1} K^{-1}	T_m[b] / K	ΔH / kJ mol^{-1}	ΔS / J mol^{-1} K^{-1}
1.0	279	4.4	16	–	–	–
	288	4.1	14			
1.1	276	8.5	31	–	–	–
1.2	268	3.4	13	372	0.5	1.2
1.3	–	–	–	269	2.4	8.9
1.4	–	–	–	268	2.7	9.9
1.5	–	–	–	261	2.2	8.4
1.6	–	–	–	262	2.5	9.6
1.7	–	–	–	259	2.3	8.8
1.8	261	2.2	8.3	274	0.41	1.5
1.9	232	7.0	30	298	0.79	2.7
	253	2.0	7.8			
2.0[c]	236	9.9	42	303	0.64	2.0
2.1	197	1.9	9.7	281	0.86	3.1
	227	5.5	24			
2.2	198	3.1	15	249	0.64	2.6
	218	4.8	22			
2.3	196	4.6	24	236	0.54	2.3
	210	3.6	17			

[a] Solid–solid phase transition temperature. [b] Melting point. [c] Ref. 18.

The differential scanning calorimetric (DSC) curves of EMPyr(FH)$_n$F ($1.0 \le n \le 2.3$) in the heating process are shown in Fig. 2 (see Fig. S3 for a magnified view of the curves around the melting points of EMPyr(FH)$_n$F ($1.8 \le n \le 2.3$)). The corresponding transition temperatures, and changes in enthalpy and entropy are summarized in Table 1. The plot of DSC transitions for the EMPyr(FH)$_n$F system based on Figs. 2 and S3 is shown in Fig. 3, where each phase has been identified with the aid of XRD analysis described below. The IPC (I) and (II) phases in Fig. 3 appear as a mesophase between crystal and liquid phases, and the phase transitions from and to these phases in this plot do not satisfy the phase rule. This can be explained by introducing another phase, not observed experimentally, between the two phases (e.g., between IPC (I) and IL). Such two-phase regions have also been observed in previously reported cases of organic plastic crystals.[33-35]

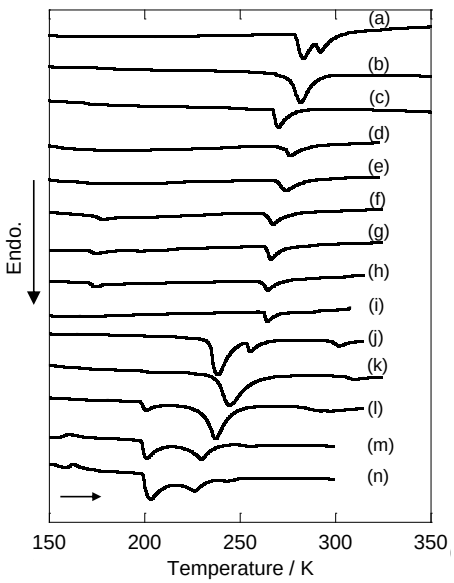

Fig. 2 Differential scanning calorimetric curves for EMPyr(FH)$_n$F in the range of $1.0 \le n \le 2.3$; n = (a) 1.0, (b)1.1, (c) 1.2, (d) 1.3, (e) 1.4, (f) 1.5, (g) 1.6, (h) 1.7, (i) 1.8, (j) 1.9, (k) 2.0, (l) 2.1, (m) 2.2, and (n) 2.3.

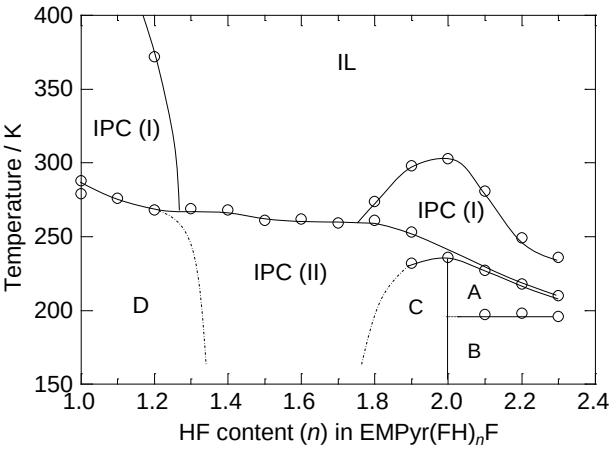

Region A: IPC (II) + EMPyr(FH)$_2$F (c)
Region B: EMPyr(FH)$_2$F (c) + EMPyr(FH)$_3$F (c)
Region C: IPC (II) + EMPyr(FH)$_2$F (c)
Region D: IPC (II) + EMPyr(FH)$_1$F (c)

Fig. 3 Plot of the DSC transitions for the EMPyr(FH)$_n$F system. IL: ionic liquid phase; IPC (I): ionic plastic crystal phase (I); IPC (II): ionic plastic crystal phase (II); EMPyr(FH)$_1$F (c): crystal phase of EMPyr(FH)$_1$F; EMPyr(FH)$_2$F (c): crystal phase of EMPyr(FH)$_2$F; EMPyr(FH)$_3$F (c): crystal phase of EMPyr(FH)$_3$F.

The XRD patterns of the IPC (I) phase for EMPyr(FH)$_n$F in the different HF content ranges ($1.0 \le n \le 1.2$ and $1.8 \le n \le 2.3$) are shown in Fig. 4. The experimental and calculated d values with indices are listed in Table S1. Only three XRD diffraction peaks are observed in the low 2θ-angle region for all the cases, and similar peaks were observed for the IPC phase of EMPyr(FH)$_{2.0}$F in a previous report.[18] This phase is indexable as the NaCl-type lattice with the indices of 111, 200, and 220, and the component ions are considered to be freely rotating in the plastic crystal phase. According to the radius ratio rule, (FH)$_n$F$^-$ is believed to occupy the octahedral sites of closely packed EMPyr$^+$ cations regardless of n.[18] The same discussion has previously been reported for the P$_{2222}$(FH)$_2$F plastic crystal although the compound belongs to a different structural type, albeit with the same coordination number of 6: EMPyr(FH)$_n$F belongs to the NaCl-type structure and P$_{2222}$(FH)$_2$F does to the inverse NiAs-type structure.[36] The lattice constants of the NaCl-type IPC (I) phase of EMPyr(FH)$_n$F as a function of n are shown in Fig. 5. The difference in the lattice constants between the two HF content ranges ($1.0 \le n \le 1.2$ and $1.8 \le n \le 2.3$) is owing to the different sizes of FHF$^-$, (FH)$_2$F$^-$, and (FH)$_3$F$^-$ (calculated volumes by the MP2/aug-cc-pVTZ calculation are 47 Å^3 for FHF$^-$, 63 Å^3 for (FH)$_2$F$^-$, and 84 Å^3 for (FH)$_3$F$^-$)[37]. In the HF content ranges ($1.0 \le n \le 1.2$ and $1.8 \le n \le 2.3$), a slight increase in the lattice constant was observed with increasing n. This behavior indicates that IPC (I) forms a mixed crystal system with a NaCl-type structure over a wide range of n. It also suggests that (FH)$_n$F$^-$ anions of more than one kind are randomly distributed in octahedral sites formed by cubic close packing of the cations. Further discussion on this point will be made in the section of DMPyr(FH)$_n$F below, because it has wider range of n values for the NaCl-type structure.

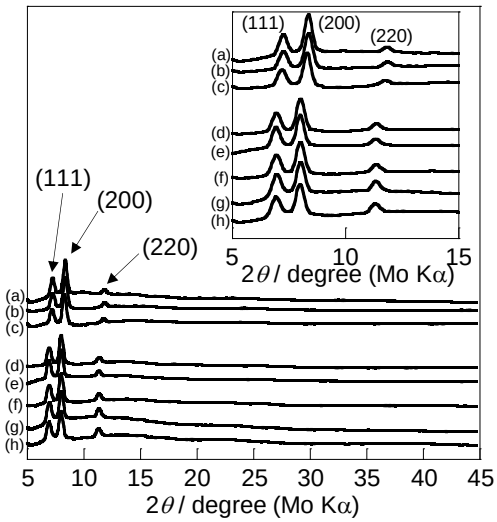

Fig. 4 X-ray diffraction patterns of EMPyr(FH)$_n$F; (a) n = 1.0 at 298 K, (b) n = 1.1 at 298 K, (c) n = 1.2 at 298 K, (d) n = 1.9 at 273 K, (e) n = 2.0 at 263 K, (f) n = 2.1 at 243 K, (g) n = 2.2 at 243 K, and (h) n = 2.3 at 213 K.

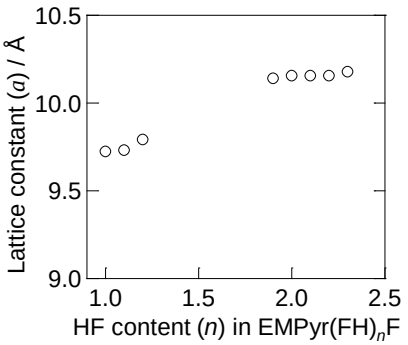

Fig. 5 The lattice constant (a) of the IPC (I) for EMPyr(FH)$_n$F calculated from the XRD patterns in Fig. 4.

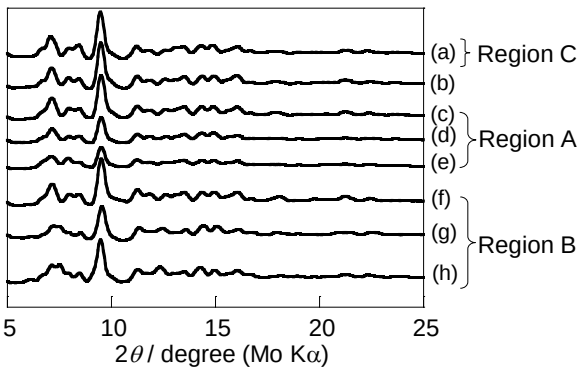

Fig. 6 X-ray diffraction patterns of EMPyr(FH)$_n$F; (a) n = 1.9 at 213 K, (b) n = 2.0 at 183 K, (c) n = 2.1 at 203 K, (d) n = 2.2 at 203 K, (e) n = 2.3 at 203 K, (f) n = 2.1 at 183 K, (g) n = 2.2 at 183 K, and (h) n = 2.3 at 183 K.

The XRD patterns of the regions A, B, and C in EMPyr(FH)$_n$F ($1.9 \leq n \leq 2.3$) are shown in Fig. 6. The patterns of regions A and C are similar and are ascribed to the crystal phase of EMPyr(FH)$_2$F. The XRD patterns of region B (Fig. 6 (g) and (h)) contain some peaks (e.g., the peak at 7.6°) in addition to peaks

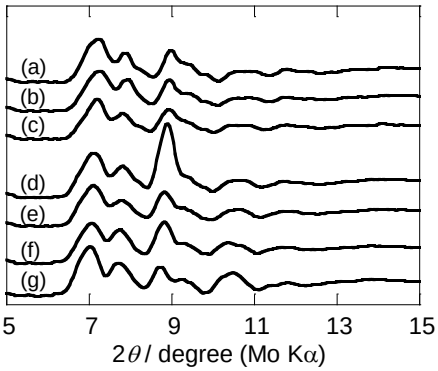

Fig. 7 X-ray diffraction patterns of EMPyr(FH)$_n$F; (a) n = 1.3 at 243 K, (b) n = 1.4 at 243 K, (c) n = 1.5 at 243 K, (d) n = 1.6 at 243 K, (e) n = 1.7 at 243 K, (f) n = 1.8 at 243 K, and (g) n = 1.9 at 238 K.

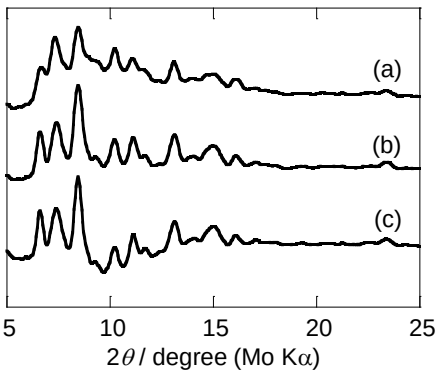

Fig. 8 X-ray diffraction patterns of EMPyr(FH)$_n$F in the range of $1.0 \leq n \leq 1.2$ at 243 K; n = (a) 1.0, (b) 1.1, and (c) 1.2.

attributed to the crystal phase of EMPyr(FH)$_2$F. The results of DSC and XRD analyses suggest that these additional peaks in the region B can be assigned to another phase with larger n value. This is probably the c rystal phase of EMPyr(FH)$_3$F by analogy with previously reported fluorohydrogenate salts, although the peaks are not clear in Fig. 6 (f) because of the small amounts of EMPyr(FH)$_3$F.[25-29] The phase transition from region B to region A corresponds to the transformation from EMPyr(FH)$_3$F crystal to IPC (II). The existence of IPC (II) in region A is based on the fact that IPC (II) appears clearly in the supercooled state (see Supporting information S-1 for the difference in thermal behavior between the cooling and heating scans). Considering that IPC (II) appears over a wide range of HF content ($1.3 \leq n \leq 1.9$), it probably coexists with the EMPyr(FH)$_2$F crystal in region A.

The XRD patterns of EMPyr(FH)$_n$F ($1.3 \leq n \leq 1.9$) at around 243 K are shown in Fig. 7. The crystal phase of EMPyr(FH)$_2$F was not observed, and the phase observed in this region is called IPC (II). The XRD pattern of IPC (II) is different from that of IPC (I), and the entropy of fusion for the IPC (II) phase (8–10 J K^{-1} mol^{-1}) is higher than those for the IPC (I) phase (1–3 J K^{-1} mol^{-1}). Nonetheless, both these values are small enough to be regarded as IPCs. It is currently unable to index the X-ray diffraction pattern of IPC (II); however the IPC (II) lattice seems to belong to a less symmetrical crystal system compared to IPC (I), which belongs to a cubic system. As in the case of IPC (I), the XRD peaks of IPC (II) gradually shift to higher angles with decreasing n, indicating that IPC (II) is an IPC with (FH)$_n$F$^-$ (n =

1 and 2) randomly occupying anion sites over a wide range of HF content.

The XRD patterns of EMPyr(FH)$_n$F in region D at 243 K (Fig. 3, $1.0 \le n \le 1.2$) are shown in Fig. 8. The patterns are different from those observed above (IPC (I), IPC (II) and regions A, B, and C). The pattern (a) in Fig. 8 corresponds to the EMPyr(FH)$_{1.0}$F crystal. The XRD patterns (b) and (c) in Fig. 8 resemble that of (a) suggesting that EMPyr(FH)$_{1.1}$F and EMPyr(FH)$_{1.2}$F contain EMPyr(FH)$_1$F crystals as the main component in this temperature range. The minor component in the mixtures with non-integer n values of 1.1 and 1.2 in region D is most likely to be IPC (II); unfortunately, this was not clear from the XRD patterns.

Thermal and structural properties of DMPyr(FH)$_n$F

The DSC curves of DMPyr(FH)$_n$F ($1.0 \le n \le 2.0$) in the heating process are shown in Fig. 9, and the corresponding transition temperatures, and changes in enthalpy and entropy are summarized in Table 2. The plot of DSC transitions for the DMPyr(FH)$_n$F system is shown in Fig. 10. The melting point of the DMPyr(FH)$_n$F system increases with decreasing n; however, no melting was observed for $n \le 1.5$, because thermal decomposition occurs below the melting point (see Fig. S6 for TG analysis of DMPyr(FH)$_1$F).

The XRD patterns of the solid phase at 298 K for DMPyr(FH)$_n$F ($1.0 \le n \le 2.0$) are shown in Fig. 11. The experimental and calculated d values with indices are listed in Table S2. Like DMPyr(FH)$_{2.0}$F,[18] this phase also has an NaCl-type structure, which is referred to as the IPC (I') phase (the prime in IPC (I') is added to distinguish this phase from the IPC (I) phase of the EMPyr(FH)$_n$F system). Unlike the XRD patterns of the IPC (I) phase of EMPyr(FH)$_n$F (Fig. 4), DMPyr(FH)$_n$F with low HF content gives weak diffraction peaks

Table 2 Summary of the DSC analyses for DMPyr(FH)$_n$F ($1.0 \le n \le 2.0$).

n	T_{s-s}[a] / K	ΔH / kJ mol^{-1}	ΔS / J mol^{-1} K^{-1}	T_m[b] / K	ΔH / kJ mol^{-1}	ΔS / J mol^{-1} K^{-1}
1.0	246	8.1	33	–	–	–
1.1	243	8.8	36	–	–	–
1.2	234	7.4	31	–	–	–
1.3	235	7.7	33	–	–	–
1.4	235	7.6	32	–	–	–
1.5	230 235	1.3 5.2	5.4 22	–	–	–
1.6	241	7.4	31	422	–	–
1.7	242	11	47	364	1.9	5.2
1.8	233 245	0.68 12	2.9 51	351	1.5	4.3
1.9	251	14	58	338	1.6	4.6
2.0[c]	258	15	57	325	1.3	4.1

[a] Solid–solid phase transition temperature. [b] Melting point. [c] Ref. 18.

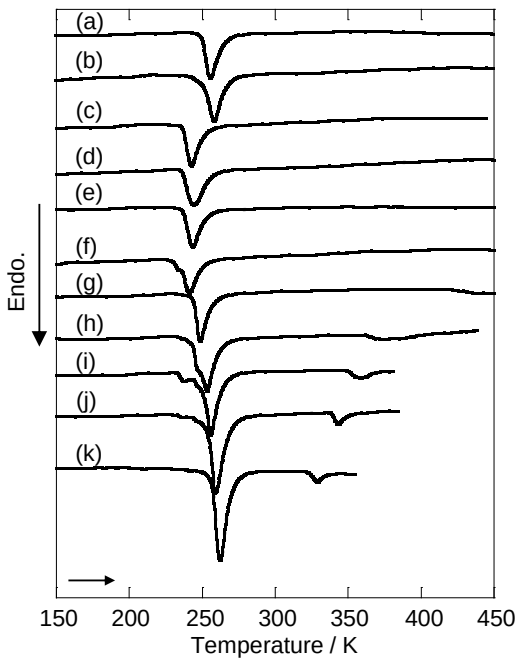

Fig. 9 Differential scanning calorimetric curves for DMPyr(FH)$_n$F in the range of $1.0 \le n \le 2.0$; n = (a) 1.0, (b)1.1, (c) 1.2, (d) 1.3, (e) 1.4, (f) 1.5, (g) 1.6, (h) 1.7, (i) 1.8, (j) 1.9, and (k) 2.0.

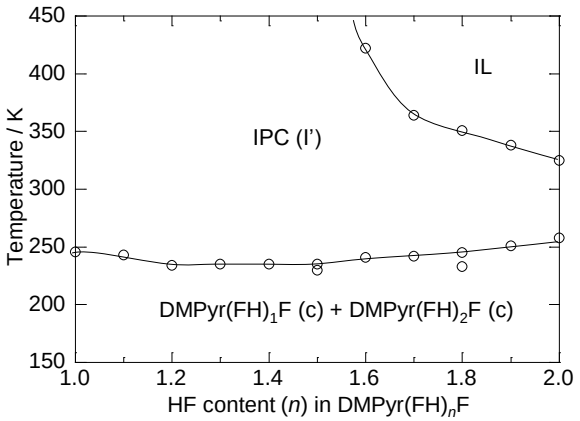

Fig. 10 Plot of the DSC transitions for the DMPyr(FH)$_n$F system. IL: ionic liquid phase; IPC (I'): ionic plastic crystal phase (I'); DMPyr(FH)$_1$F (c): crystal phase of DMPyr(FH)$_1$F; and DMPyr(FH)$_2$F (c): crystal phase of DMPyr(FH)$_2$F.

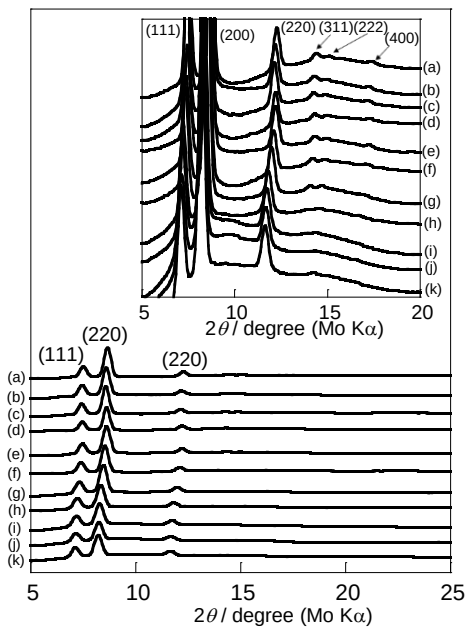

Fig. 11 X-ray diffraction patterns of DMPyr(FH)$_n$F in the range of $1.0 \le n \le 2.0$ at 298 K; n = (a) 1.0, (b)1.1, (c) 1.2, (d) 1.3, (e) 1.4, (f) 1.5, (g) 1.6, (h) 1.7, (i) 1.8, (j) 1.9, and (k) 2.0.

with indices of 311, 222, and 400 in addition to 111, 200, and 220. This probably results from the better crystal packing and lower thermal factor for each atom in the lattice of DMPyr(FH)$_n$F compared to those in the lattice of EMPyr(FH)$_n$F. These 6 peaks were observed even at higher temperatures of 373 and 443 K, as shown in Fig. S7. The lattice constant a of IPC (I') as a function of n is shown in Fig. 12. The a value does not vary significantly in the region $1.0 \leq n \leq 1.5$, whereas it increases with n in the region $1.6 \leq n \leq 2.0$. This behavior probably arises from an increase in the motion of anions with an increase of n, i.e., an increase of $(FH)_2F^-$ with respect to $(FH)_1F^-$, which is reflected in a decrease in the intensity of the 311, 222, and 400 peaks for DMPyr(FH)$_n$F in the region $n > 1.5$. The same behavior is also observed for EMPyr(FH)$_n$F although the IPC (I) phase does not appear in the range of $1.3 \leq n \leq 1.9$ (Figs. 3 and 5).

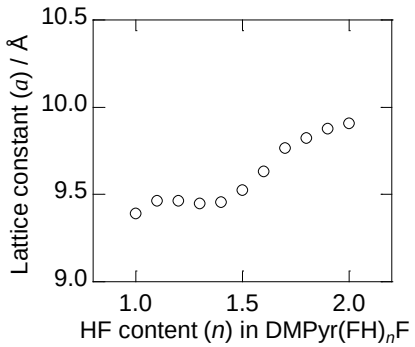

Fig. 12 The lattice constant (a) of the IPC (I') for DMPyr(FH)$_n$F ($1.0 \leq n \leq 2.0$) calculated from the XRD patterns in Fig. 11.

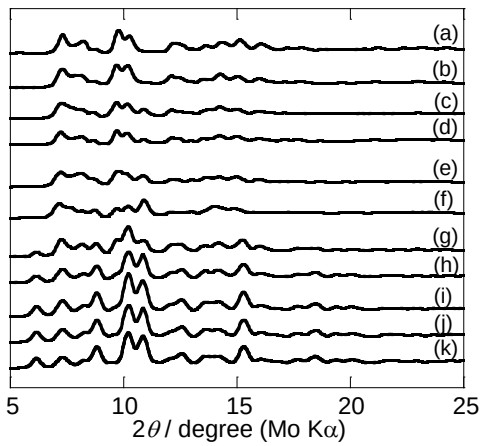

Fig. 13 X-ray diffraction patterns of DMPyr(FH)$_n$F in the range of $1.0 \leq n \leq 2.0$ at 203 K; (a) 1.0, (b)1.1, (c) 1.2, (d) 1.3, (e) 1.4, (f) 1.5, (g) 1.6, (h) 1.7, (i) 1.8, (j) 1.9, and (k) 2.0.

The XRD patterns of the phase observed at 203 K for DMPyr(FH)$_n$F ($1.0 \leq n \leq 2.0$) are shown in Fig. 13. The DMPyr(FH)$_1$F and DMPyr(FH)$_2$F crystals have different XRD patterns, and the XRD patterns of DMPyr(FH)$_n$F in the range $1.1 \leq n \leq 1.9$ are composed of peaks attributable to both these salts, indicating that DMPyr(FH)$_n$F ($1.1 < n < 1.9$) is a mixture of these two crystal phases in the low temperature region. There are several peaks that are obviously attributable to DMPyr(FH)$_1$F or DMPyr(FH)$_2$F in the patterns of DMPyr(FH)$_n$F ($1.1 < n < 1.9$); the peaks at $2\theta = 9.8$, 12.2, and 15.2° for DMPyr(FH)$_1$F and those at $2\theta = 6.2$, 8.8, 10.9, 12.6, and 15.4° for DMPyr(FH)$_2$F. The small peaks and shoulders are observed around 230 – 240 K in the DSC curves for DMPyr(FH)$_n$F (Fig. 9 (f), (h), and (i)) in addition to the main peak. By taking into account the results of XRD analysis, they could be attributed to the phase transition from the two-phase region of DMPyr(FH)$_1$F and DMPyr(FH)$_2$F crystals to a two-phase region of IPC (I') and DMPyr(FH)$_2$F crystal, as seen in the reports for the organic plastic crystals with two-phase regions of crystal and plastic crystal phases.[33-35] Detailed analysis on this point is difficult at the current stage because the two transition are too close to each other.

The phase diagram of the EMPyr(FH)$_n$F system is more complicated than that of DMPyr(FH)$_n$F. As described in a previous study,[18] all the $DMPyr^+$ cations in DMPyr(FH)$_2$F are immobilized in the IPC(I') lattice framework. In contrast, some $EMPyr^+$ cations are mobile in the IPC (I) of EMPyr(FH)$_{2.0}$F, whereas the remaining $EMPyr^+$ cations are fixed to the crystal lattice framework. In addition to the differences in symmetry, the motion of cations may give rise to the different thermal behavior of EMPyr(FH)$_n$F and DMPyr(FH)$_n$F systems.

Conclusions

The effects of HF content n in EMPyr(FH)$_n$F ($1.0 \leq n \leq 2.3$) and DMPyr(FH)$_n$F ($1.0 \leq n \leq 2.0$) on their thermal and structural properties have been investigated. In the EMPyr(FH)$_n$F system, several solid phases (IPC (I) and IPC (II) phases, and crystal phases of EMPyr(FH)$_1$F, EMPyr(FH)$_2$F, and EMPyr(FH)$_3$F) were observed. The IPC (I) phase has an NaCl-type structure and contains $(FH)_nF^-$ (n = 1, 2, and 3) randomly occupying the anion sites in the lattice. The melting point of EMPyr(FH)$_n$F in the range $1.8 \leq n \leq 2.3$ becomes maximal at $n = 2.0$, is nearly constant around 260–270 K for $1.3 \leq n \leq 1.7$, and increases with decreasing HF content when $1.0 \leq n \leq 1.2$. In the DMPyr(FH)$_n$F system, the IPC (I') and crystal phases of DMPyr(FH)$_1$F and DMPyr(FH)$_2$F were observed. The IPC (I') phase of DMPyr(FH)$_n$F has structural features similar to those of IPC (I) of EMPyr(FH)$_n$F, but the motion of ions in IPC (I') is more restricted than in IPC (I). Melting point increases monotonously with decreasing HF content.

The dialkylpyrrolidinium fluorohydrogenate salts studied in this paper show thermal behavior significantly different from dialkylimidazolium fluorohydrogenate salts, which do not exhibit the IPC phase over a wide range of n values.[25,26] The relatively spherical shape of dialkylpyrrolidinium cations facilitates the disordering of the cation in the crystal lattice, which leads to the formation of the IPC phases.

Acknowledgements

The authors would like to thank the Hattori Hokokai Foundation for financially supporting this work.

Notes and References

Graduate School of Energy Science, Kyoto University, Yoshida, Sakyo-ku, Kyoto, 606-8501, Japan. Fax: +81-75-753-5906; Tel: +81-75-753-4817; E-mail: k-matsumoto@energy.kyoto-u.ac.jp

† Electronic Supplementary Information (ESI) available: IR spectra, X-ray powder diffraction data, DSC curves, and additional discussion. See DOI: 10.1039/b000000x/

‡ Footnotes should appear here. These might include comments relevant to but not central to the matter under discussion, limited experimental and spectral data, and crystallographic data.

1. D. R. MacFarlane, J. Huang and M. Forsyth, *Nature*, 1999, **402**, 792–794.
2. H.-B. Han, J. Nie, K. Liu, W.-K. Li, W.-F. Feng, M. Armand, H. Matsumoto and Z.-B. Zhou, *Electrochim. Acta*., 2010, **55**, 1221–1226.
3. D. R. MacFarlane, P. Meakin, N. Amini and M. Forsyth, *J. Phys.: Condens. Matter*, 2001, **13**, 8257–8267.
4. L. Jin, K. M. Nairn, C. M. Forsyth, A. J. Seeber, D. R. MacFarlane, P. C. Howlett, M. Forsyth and J. M. Pringle, *J. Am. Chem. Soc.*, 2012, **134**, 9688–9697.
5. Z.-B. Zhou and H. Matsumoto, *Electrochem. Commun*., 2007, **9**, 1017–1022.
6. U. A. Rana, M. Forsyth, D. R. MacFarlane and J. M. Pringle, *Eletrochim. Acta*, 2012, **84**, 213–222.
7. J. M. Pringle, *Phys. Chem. Chem. Phys*., 2013, **15**, 1339–1351.
8. J. M. Pringle, P. C. Howlett, D. R. MacFarlane and M. Forsyth, *J. Mater. Chem*., 2010, **20**, 2056–2062.
9. J. Timmermans, *J. Phys. Chem. Solids*, 1961, **18**, 1–8.
10. D. R. MacFarlane, P. Meakin, J. Sun, N. Amini and M. Forsyth, *J. Phys. Chem. B*, 1999, **103**, 4164–4170.
11. D. R. MacFarlane and M. Forsyth, *Adv. Mater*., 2001, **13**, 957–966.
12. N. A. Choudhury, S. Sampath and A. K. Shukla, *Energy Environ. Sci*., 2009, **2**, 55–67.
13. J. Fuller, A. C. Breda and R. T. Carlin, *J. Electrochem. Soc*., 1997, **144**, L67–L70.
14. A. Lewandowski and A. Świderska, *Solid State Ionics*, 2003, **161**, 243–249.
15. M. Forsyth, J. Huang and D. R. MacFarlane, *J. Mater. Chem*., 2000, **10**, 2259–2265.
16. P.-J. Alarco. Y. Abu-Lebdeh, N. Ravet and M. Armand, *Solid State Ionics*, 2004, **172**, 53–56.
17. P.-J. Alarco. Y. Abu-Lebdeh and M. Armand, *Solid State Ionics*, 2004, **175**, 717–720.
18. R. Taniki, K. Matsumoto, R. Hagiwara, K. Hachiya, T. Morinaga and T. Sato, *J. Phys. Chem. B*, 2013, **117**, 955–960.
19. R. Taniki, K. Matsumoto, T. Nohira and R. Hagiwara, *J. Power Sources*, in press [10.1016/j.jpowsour.2013.07.020].
20. G. Zabinska, P. Ferloni and M. Sanesi, *Thermochim. Acta*, 1987, **122**, 87–94.
21. V. Armel, D. Velayutham, J. Sun, P. C. Howlett, M. Forsyth, D. R. MacFarlane and J. M. Pringle, *J. Mater. Chem*., 2011, **21**, 7640–7650.
22. M. Moriya, D. Kato, W. Sakamoto and T. Yogo, *Chem. Commun*., 2011, **47**, 6311–6313.
23. Z.-B. Zhou, H. Matsumoto and K. Tatsumi, *Chem. Eur. J*., 2005, **11**, 752–766.
24. K. Matsumoto, J. Ohtsuki, R. Hagiwara and S. Matsubara, *J. Fluorine Chem*., 2006, **127**, 1339–1343.
25. R. Hagiwara, Y. Nakamori, K. Matsumoto and Y. Ito, *J. Phys. Chem. B*, 2005, **109**, 5445–5449.
26. F. Xu, K. Matsumoto and R. Hagiwara, *J. Phys. Chem. B*, 2012, **116**, 10106–10112.
27. G. H. Cady, *J. Am. Chem. Soc*., 1934, **56**, 1431–1434.
28. B. Boinon, A. Marchand and R. Cohen-Adad, *J. Therm. Anal*., 1976, **10**, 411–418.
29. R. V. Winsor and G. H. Cady, *J. Am. Chem. Soc*., 1948, **70**, 1500–1502.
30. I. Gennick, K. M. Harmon and M. M. Potvin, *Inorg. Chem*., 1977, **16**, 2033–2040.
31. R. Hagiwara, K. Matsumoto, Y. Nakamori, T. Tsuda, Y. Ito, H. Matsumoto and K. Momota, *J. Electrochem. Soc*., 2003, **150**, D195–D199.
32. RAPID XRD, version 2.3.3; Rigaku coorporation: Tokyo, Japan, 1999.
33. D. Chandra, W. Ding, R. A. Lynch and J. J. Tomilinson, *J. Less–Common Met*., 1991, **168**, 159–167.
34. J. Salud, D. O. López, M. Barrio, J. L. Tamarit, H. A. J. Oonk, P. Negrier and Y. Haget, *J. Solid State Chem*., 1997, **133**, 536–544.
35. R. Russell, R. Chellappa and D. Chandra, *CALPHAD: Comput. Coupling Phase Diagrams Thermochem*., 2004, **28**, 41–48.
36. T. Enomoto, S. Kanematsu, K. Tsunashima, K. Matsumoto and R. Hagiwara, *Phys. Chem. Chem. Phys.* 2011, **13**, 12536–12544.
37. T. Enomoto, Y. Nakamori, K. Matsumoto and R. Hagiwara, *J. Phys. Chem. C*, 2011, **115**, 4324–4332.